Transport effects in remote-doped InSb/$Al_xIn_{1-x}Sb$ heterostructures

2010 New J. Phys. 12 053022

(http://iopscience.iop.org/1367-2630/12/5/053022)

New Journal of Physics
The open-access journal for physics

Transport effects in remote-doped InSb/$Al_xIn_{1-x}Sb$ heterostructures

O J Pooley[1,2], A M Gilbertson[3], P D Buckle[1,4], R S Hall[1], L Buckle[1], M T Emeny[1], M Fearn[1], L F Cohen[3] and T Ashley[1]

[1] QinetiQ, St Andrews Road, Malvern, Worcestershire WR14 3PS, UK
[2] Photon Science Institute, University of Manchester, Alan Turing Building, Manchester M13 9PL, UK
[3] Department of Physics, Imperial College, Prince Consort Road, London SW7 2BZ, UK
E-mail: p.buckle@qinetiq.com

New Journal of Physics **12** (2010) 053022 (9pp)
Received 19 January 2010
Published 14 May 2010
Online at http://www.njp.org/
doi:10.1088/1367-2630/12/5/053022

Abstract. Low- and high-field magnetotransport measurements on two 30 nm δ-doped InSb/AlInSb quantum wells (QWs) with different doping densities are reported. The QW two-dimensional electron gas (2DEG) carrier densities and mobilities were extracted by analysis of the Hall and quantum Hall data, mobility spectra and Shubnikov-de Haas oscillations. 2DEG channel mobilities of up to 324 000 $cm^2\,V^{-1}\,s^{-1}$ ($T = 2$ K) and 44 000 $cm^2\,V^{-1}\,s^{-1}$ ($T = 300$ K) are extracted. Carrier densities and mobilities for transport parallel to the 2DEG layer are also deduced where observable. The importance of thermally generated carriers in the lower AlInSb barrier material and the role of transport within the δ-doping plane is considered and the total carrier population as a function of temperature of the two samples is deduced, which is in excellent agreement with experimental observation.

[4] Author to whom any correspondence should be addressed.

Contents

1. Introduction

Narrow band gap semiconductors are exciting candidates for high-speed electronics [1, 2], quantum devices [3, 4], ballistic transport [5] and spintronic applications [6]. Modulation-doped heterostructures provide the high-mobility samples that are required for these applications. Of the III–V semiconductors, InSb has the lightest effective mass ($0.014m_e$) and narrowest band gap (170 meV at room temperature) along with a large dielectric constant ($16.8\epsilon_0$) and an exceptionally large Landé g-factor (~ -51) [7]. This makes the InSb/AlInSb system a particularly interesting candidate for these applications. The various challenges faced in heavily mismatched epitaxial growth have meant that development in the understanding of these systems is still at a relatively immature stage compared to wider gap III–V semiconductor systems such as GaAs or GaN.

In this paper, we present the growth and magnetotransport measurements of two high-quality InSb/$Al_xIn_{1-x}Sb$ modulation-doped heterostructures with different doping densities. The lower-doped sample is shown to exhibit single carrier conduction at low temperature (2 K), with the onset of parallel conduction at higher temperature, while the higher-doped sample shows a parallel conduction at low and high temperatures. In both cases, the mobility of the 2D carrier is extracted.

2. Sample preparation and measurements

Two InSb/$Al_xIn_{1-x}Sb$ heterostructures of identical compositional design (shown schematically in figure 1) but different doping densities were grown by molecular beam epitaxy (MBE) using standard effusion cells for the In, Ga and Al and cracker cells for the Sb and As, at a nominal growth rate of 1 μm h^{-1}. The 30 nm wide InSb quantum wells (QWs) were surrounded by an AlInSb matrix. The top 50 nm barrier of $Al_{0.15}In_{0.85}Sb$ contained the Te delta-doping plane. The lower $Al_{0.10}In_{0.9}Sb$ barrier was 3 μm thick and grown with a nominal n-type background doping of 1×10^{15} cm^{-3} at room temperature. This was separated from the GaAs cleaned and buffered substrate surface by 200 nm AlSb. Secondary Ion Mass Spectrometry (SIMS) studies on similar layers to these have shown the Te dopant ions to be distributed through the top cap above the nominal point of introduction [8]. This is illustrated in figure 1 by the solid points.

Samples were processed into Hall bars with shallow ohmic contacts. Low-field measurements ($0 \leqslant B \leqslant 350$ mT) were performed in a helium bath cryostat between 4.5 and 300 K. High-field measurements ($-7.5\,T \leqslant B \leqslant 7.5\,T$), using a low-frequency lock-in technique, were performed in a cryogen-free magnet system, between 2 and 290 K. The

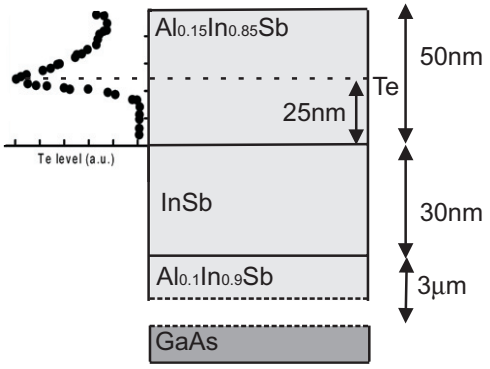

Figure 1. Schematic diagram of the heterostructure growth. The data to the left represent the SIMS profile measured for the Te dopant.

extraction of carrier concentrations is discussed in section 3. Sample 1 had a total carrier concentration (n_{tot}) of $15.2 \times 10^{11}\,\mathrm{cm}^{-2}$ ($16.4 \times 10^{11}\,\mathrm{cm}^{-2}$) at 2 K (290 K). Sample 2 had n_{tot} of $1.9 \times 10^{11}\,\mathrm{cm}^{-2}$ ($10.4 \times 10^{11}\,\mathrm{cm}^{-2}$) at 2 K (290 K).

3. Results and discussion

Figures 2(a) and (b) show the high-field magnetoresistivity (ρ_{xx}) and Hall resistivity (ρ_{xy}) of samples 1 and 2, respectively, measured at 2 K. Sample 2 shows distinct, single-period Shubnikov de-Haas (SdH) oscillations in ρ_{xx} and well-developed quantum Hall plateaux in ρ_{xy}, which have previously been observed in samples of this type [9, 10]. In stark contrast, ρ_{xx} data for sample 1 show SdH oscillations superposed on a significant background signal with negligible structure observed in the ρ_{xy} data. It is noteworthy that the SdH oscillations remain single period in $1/B$. The background contribution to ρ_{xx} is a clear indication of significant parallel charge transport elsewhere in the device. Assuming that the SdH oscillations originate from the ground state subband in the QW, the periodicity in $1/B$ can be used to determine the carrier density of the two-dimensional electron gas (n_{2DEG}). For sample 1, this was $3.5 \times 10^{11}\,\mathrm{cm}^{-2}$ and for sample 2, $1.9 \times 10^{11}\,\mathrm{cm}^{-2}$.

The gradient of the slope of ρ_{xy} at high field, bisecting quantum Hall plateaux where they exist, gives a good approximation to n_{tot} [11]. In sample 2 at low temperature, this is in excellent agreement with the concentration calculated by the period of the SdH oscillations. However, in sample 1, the total carrier density is significantly greater than n_{2DEG}. This can be used to calculate the density of the parallel carrier ($n_{\parallel}$) by

$$n_{\mathrm{tot}} = n_{\mathrm{2DEG}} + n_{\parallel}. \tag{1}$$

For sample 1, the mobilities of the individual carriers were calculated from fits of the ρ_{xy} data to a two-carrier model [12]. The model provides an excellent fit to the experimental data for ρ_{xy}, as shown by figure 3(a) for sample 1. At 2 K, the mobilities of the two-carriers in sample 1 were found to be $324\,000\,\mathrm{cm}^2\,\mathrm{V}^{-1}\,\mathrm{s}^{-1}$ for the 2D carrier contribution and $4000\,\mathrm{cm}^2\,\mathrm{V}^{-1}\,\mathrm{s}^{-1}$ for the parallel carrier contribution. The second carrier has a concentration of $11.7 \times 10^{11}\,\mathrm{cm}^{-2}$. The effective average mobility extracted from the model was $74\,500\,\mathrm{cm}^2\,\mathrm{V}^{-1}\,\mathrm{s}^{-1}$. This is in good agreement with the measured mobility of $74\,000\,\mathrm{cm}^2\,\mathrm{V}^{-1}\,\mathrm{s}^{-1}$, extracted from the high-field

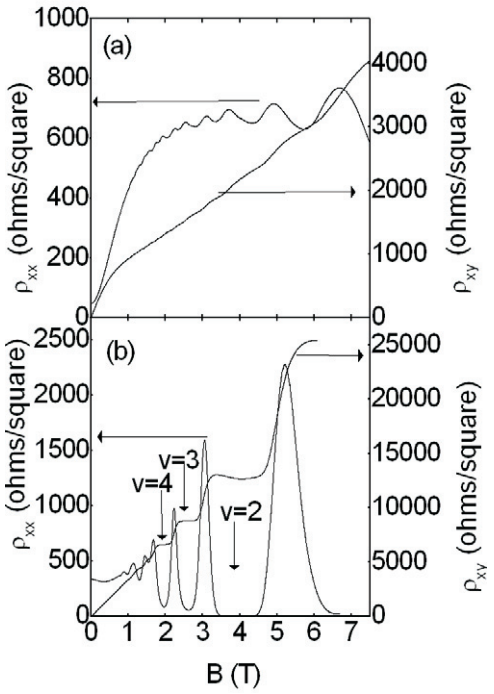

Figure 2. (a) High-field magnetoresistivity (ρ_{xx}) and Hall resistivity (ρ_{xy}) of sample 1. ρ_x shows single-period SdH oscillations with a significant background. (b) ρ_x and ρ_{xy} of sample 2. ρ_{xx} again shows single-period SdH oscillation, with no background indicating single-carrier behaviour. ρ_{xy} shows quantum Hall plateaux. Both sets of data taken at 2 K.

gradient of ρ_{xy}. When the SdH oscillations are no longer observable both carrier concentrations are extracted from the two-carrier model.

To give further confidence in this analysis, we have used mobility spectra analysis on low-field data. The resistivity data were corrected for the measured length/width ratio of the Hall bars. The mobility spectrum from the magnetoresistance and Hall coefficient data, after conversion to the conductivity tensor components, were calculated using a matrix inversion approach similar to the formalism of Beck and Anderson [13]. At low temperature the magnetic fields used were limited to those below which the quantum Hall effect might produce small but significant (when looking for a second carrier) oscillations in the magnetoresistance or Hall coefficient ($\leqslant$0.4 T). The matrix inversion approach is known to be susceptible to ill-conditioned matrices. The robustness of the spectra produced were checked by permuting a selected set of experimental data points and removing data permutations producing solutions that were inconsistent with the most common number and nature of carriers (i.e. *n*-type). Data point permutations that produced peaks at zero mobility, or balanced mobility peaks at unphysical, large, positive and negative values (unphysical compensation) were ignored. Generally, the mobility spectra in these samples yielded two well-resolved *n*-type mobility peaks. In the fitting procedure, the mobility of the 2nd (high mobility) carrier peak in the spectrum was initially fixed. The remaining parameters (peak conductivity of 1st and 2nd peaks and mobility of the 1st peak) were used as initial values in a two-carrier fit to the magnetoresistance and Hall coefficient

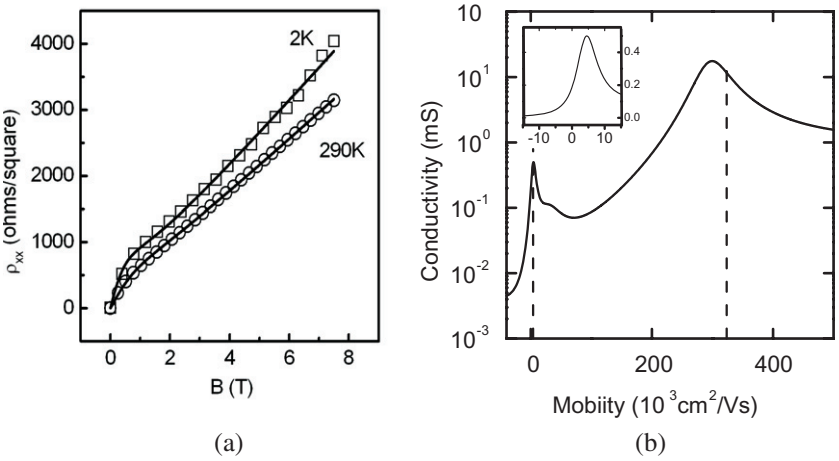

Figure 3. (a) Experimental ρ_{xy} for sample 1 at 2 and 290 K (points) with fits using the two-carrier model [12] (lines). The number of experimental points have been reduced for clarity. (b) Mobility spectra of sample 1 at 2 K. The inset shows the region around 0 $cm^2\,V^{-1}\,s^{-1}$. The dashed lines show the results obtained following the analysis shown in (a).

data. The mobility of the high mobility carrier was then allowed to vary simultaneously with the other three fitting parameters to see if a true local minimum in the fitting function had been achieved. This produced little mobility change from the original mobility spectrum. The resulting mobility spectrum of sample 1 at 2 K is shown in figure 3(b). The mobilities calculated by the analytical two-carrier model are also shown in the figure as dashed lines and show that there is extremely good agreement between the two methods of analysis.

Figure 4(a) shows a self-consistent Schrödinger–Poisson (SP) solution [14] for the conduction band of sample 1 at low temperature. This sample is heavily doped with $n_{\mathrm{tot}} = 15.6 \times 10^{11}\ \mathrm{cm}^{-2}$. Figure 4(b) shows the SP solution for sample 2, which is more lightly doped, with $n_{\mathrm{tot}} = 1.9 \times 10^{11}\ \mathrm{cm}^{-2}$. The SP solution indicates that sample 1 has four occupied levels, with the majority of carriers confined in the delta-doping region and not the QW. This is in good agreement with the multi-carrier behaviour observed in experimental data. Sample 2, has a single occupied level, which is also in good agreement with the observed magnetotransport. As the temperature is increased, the ρ_{xy} of sample 2 shows a second carrier above 140 K. At the same temperature, the SP solution shows the occupation of energy levels in the delta-doping energy minimum of the conduction band profile.

Figures 5(a) and (b) show the temperature variation of the measured mobility (lines) and the mobility of the 2D carrier (open circles) for samples 1 and 2, respectively. In both samples the mobility of the 2D carrier behaves as expected from analysis of the various scattering mechanisms present [8]. The mobility of the 2D carrier in sample 1 is relatively stable at 324 000 $cm^2\,V^{-1}\,s^{-1}$ until the temperature reaches 40 K, where phonon scattering becomes significant and the mobility reduces to 42 000 $cm^2\,V^{-1}\,s^{-1}$ by 290 K. The 2D carrier in sample 2 has a mobility of 84 000 $cm^2\,V^{-1}\,s^{-1}$ at low temperatures, which reduces to 44 000 $cm^2\,V^{-1}\,s^{-1}$ at 290 K as a result of phonon scattering. Figure 5 also shows the mobility of the parallel carriers of (a) sample 1 (open diamonds) and (b) sample 2 (filled diamonds). In sample 1, the mobility of the second (parallel) carrier is relatively temperature invariant. This suggests that it is limited

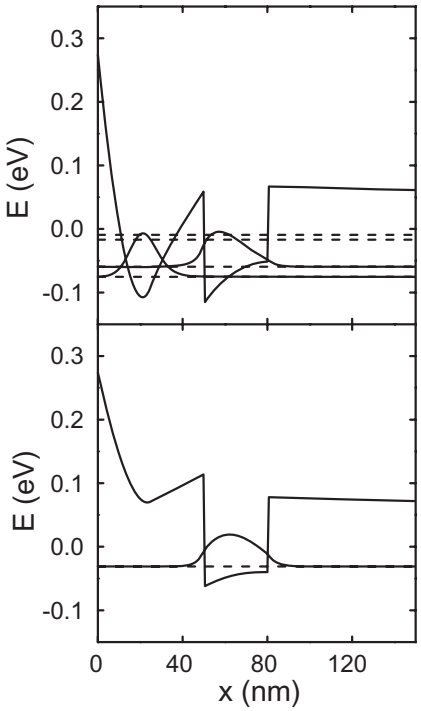

Figure 4. Self-consistent SP solutions of the conduction band of (a) sample 1 and (b) sample 2 at low temperature, showing occupied levels. The dashed lines show the energy levels, with the solid lines showing associated eigenfunctions. The axis is defined such that the Fermi level lies at 0 eV.

by a weakly temperature-dependent scattering mechanism, consistent with impurity scattering, supporting the conjecture that the parallel carrier is localized in the delta-doping plane, where the greatest density of scattering centres is located and not below the well.

Figure 6 shows the total carrier density of samples 1 and 2 (bold solid lines) as a function of temperature. In addition, for sample 2 we have included $n_{2\mathrm{DEG}}$ (open circles) and $n_{\|}$ (open diamonds), extracted from the analytical two-carrier model and the carrier density in the well (n_{QW}) and delta-doping plane (n_{doping}) extracted from the SP model (feint solid lines). It can be seen that n_{QW} provides excellent agreement with $n_{2\mathrm{DEG}}$ at all temperatures. However, when the second carrier is present, there is a large discrepancy between n_{doping} and $n_{\|}$. The difference between the two-carriers varies approximately exponentially with temperature, suggesting that thermally generated carriers (which are not considered in the SP model) strongly contribute to parallel conduction. The approximate intrinsic carrier density (n_{barrier}) was calculated for the 10% Al lower barrier. Assuming a background doping level of $1 \times 10^{15}\,\mathrm{cm}^{-3}$, the Fermi level was found to lie 115 meV below the conduction band. Using this Fermi level, n_{barrier} was then found by [15]

$$n_{\mathrm{barrier}} = N_{\mathrm{c}}\ \exp\left(-\frac{E_{\mathrm{c}} - E_{\mathrm{F}}}{kT}\right) + n_{\mathrm{background}}, \tag{2}$$

where $N_{\mathrm{c}} = 2.4 \times 10^{13}\mathrm{T}^{3/2}\,\mathrm{cm}^{-3}$ is the effective density of states in the conduction band and $n_{\mathrm{background}}$ is the electron density resulting from background doping. After conversion to a sheet density, n_{barrier} was estimated to vary between $0.6 \times 10^{11}\,\mathrm{cm}^{-2}$ at 140 K and $5.8 \times 10^{11}\,\mathrm{cm}^{-2}$

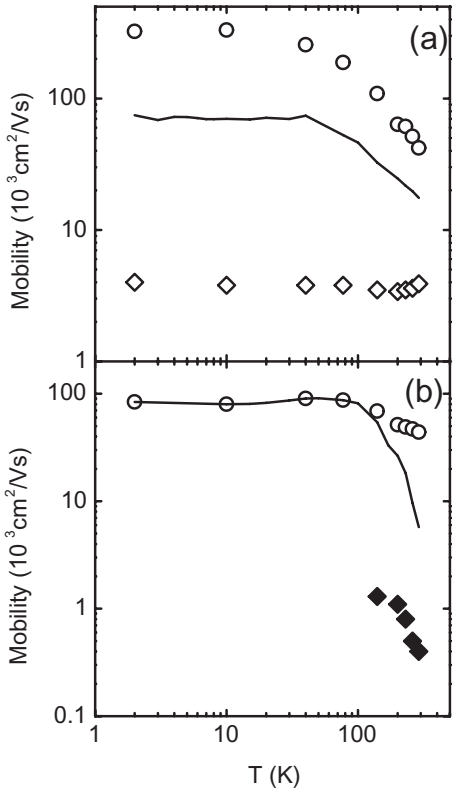

Figure 5. Temperature dependence of the mobility of 2D (open circles) carriers and the measured mobility (line) extracted from Hall data for (a) sample 1 and (b) sample 2. The parallel carrier is shown by diamonds in both cases.

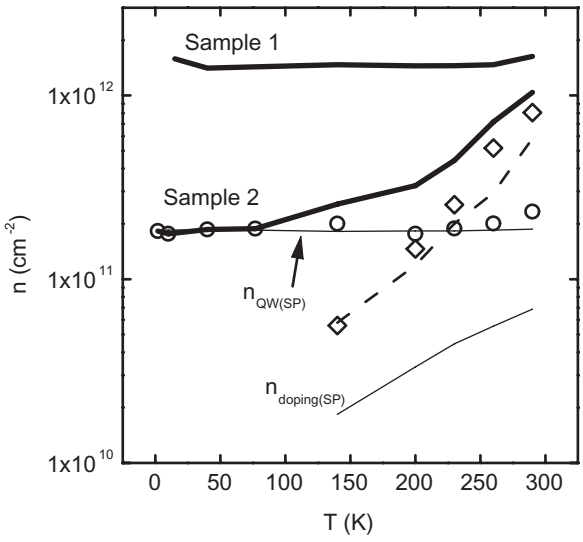

Figure 6. Carrier density of samples 1 and 2 (bold solid lines). The contributions to the density calculated from the two-carrier model—n_{2DEG} (open circles) and $n_{\|}$ (open diamonds) and calculated from the SP model (faint solid lines) are shown for sample 2, along with $n_{barrier}$ for both samples (dashed line).

at 290 K, as shown by the dashed line in figure 6. It can be seen that at lower temperatures, thermally excited carriers are a much smaller proportion of the total carrier density. $n_{\|}$ from the analytical two-carrier model is in good agreement with the sum of n_{doping} from the SP model and n_{barrier}. When added to n_{QW} from the SP model, this gives good agreement with the measured total carrier density.

The same contributions (n_{2DEG}, $n_{\|}$, n_{QW} and n_{doping}) can be calculated for sample 1. Assuming the same growth conditions, n_{barrier} is the same in samples 1 and 2, therefore the lower barrier contribution should be identical for the two samples. As can be seen in figure 6, the effect of intrinsic carriers in the lower barrier in the highly doped sample is less significant than in the lower-doped sample at high temperatures, where it is a significant proportion of the total number of carriers. These results are consistent with the entirely different temperature dependence of the mobility of the parallel carrier from samples 1 and 2.

4. Conclusion

Growth of high-quality InSb/AlInSb heterostructures has been demonstrated, with high room temperature (44 000 $\text{cm}^2\,\text{V}^{-1}\,\text{s}^{-1}$) and low temperature (324 000 $\text{cm}^2\,\text{V}^{-1}\,\text{s}^{-1}$) 2DEG mobility. Samples with both single- and two-carrier transport at low temperature have been measured. Sample 2, whilst single carrier at low temperature, becomes multiple carrier by ∼140 K. The large increase in the carrier concentration of this sample from 1.9×10^{11} to $10.4 \times 10^{11}\,\text{cm}^{-2}$ is explained by the presence of thermally generated carriers in the lower barrier, which accounts for the parallel conduction. In higher-doped samples, it is concluded that parallel conduction originates from carriers occupying the delta-doping plane.

Acknowledgments

We thank RJ Nicholas (Oxford University) for several useful discussions and P Webber (QinetiQ) for device processing. OJP and AMG acknowledge support from the UK EPSRC. We acknowledge financial support from the UK MOD Defence Technology and Innovation centre (DTIC).

References

[1] Ashley T, Emeny M, Hayes D, Hilton K, Jefferies R, MacLean J, Smith S, Tang A, Wallis D and Wilding P 2009 High-performance InSb based quantum well field effect transistors for low-power dissipation applications In *IEDM*

[2] Bennett B R, Ancona M G and Boos J B 2009 Compound semiconductors for low-power p-channel field-effect transistors *MRS Bull.* **34** 530

[3] Elzerman J M, Hanson R, Greidanus J S, Willems van Beveren L H, De Franceschi S, Vandersypen L M K, Tarucha S and Kouwenhoven L P 2003 Few-electron quantum dot circuit with integrated charge read out *Phys. Rev.* B **67** 161308

[4] Goel N, Graham J, Keay J C, Suzuki K, Miyashita S, Santos M B and Hirayama Y 2005 Ballistic transport in InSb mesoscopic structures *Physica* E **26** 455

[5] Goel N, Chung S J, Santos M B, Suzuki K, Miyashita S and Hirayama Y 2004 Ballistic transport in InSb quantum wells at high temperature *Physica* E **20** 251

[6] Gilbertson A M, Fearn M, Jefferson J H, Murdin B N, Buckle P D and Cohen L F 2008 Zero-field spin splitting and spin lifetime in n-InSb/$In_xAl_{1-x}Sb$ asymmetric quantum well heterostructures *Phys. Rev.* B **77** 165335

[7] Madelung O, Rössler U and Schulz M 2006 *Landolt and Bornstein—Group III Condensed matter: Group IV Elements, (IV–IV) and (III–V) Compounds. Part b—Electronic, Transport, Optical and Other Properties* (Berlin: Springer)

[8] Orr J M S, Gilbertson A M, Fearn M, Croad O W, Storey C J, Buckle L, Emeny M T, Buckle P D and Ashley T 2008 Electronic transport in modulation-doped InSb quantum well heterostructures *Phys. Rev.* B **77** 165334

[9] Gilbertson A M, Branford W R, Fearn M, Buckle L, Buckle P D, Ashley T and Cohen L F 2009 Zero-field spin splitting and spin-dependent broadening in high-mobility InSb/$In_xAl_{1-x}Sb$ asymmetric quantum well heterostructures *Phys. Rev.* B **79** 235333

[10] Chokomakoua J C, Goel N, Chung S J, Santos M B, Hicks J L, Johnson M B and Murphy S Q 2004 Ising quantum Hall ferromagnetism in InSb-based two-dimensional electronic systems *Phys. Rev.* B **69** 235315

[11] Reed M A, Kirk W P and Kobiela P S 1986 Investigation of parallel conduction in GaAs/Al_xGa_{1-x} modulation-doped structures in he quantum limit *IEEE J. Quantum Electron* **22** 1753

[12] Zhang T, Clowes S K, Debnath M, Bennet A, Roberts C, Harris J J, Stradling R A, Cohen L F, Lyford T and Fewster P F 2004 High-mobility thin InSb films grown by molecular beam epitaxy *Appl. Phys. Lett.* **84** 4463

[13] Beck W A and Anderson J R 1987 Determination of electrical transport properties using a novel magnetic field-dependent Hall technique *J. Appl. Phys.* **62** 541

[14] Tan I-H, Snider G L, Chang D L and Hu E L 1990 A self-consistent solution of Schrödinger–Poisson equations using a nonuniform mesh *J. Appl. Phys.* **68** 4071

[15] Sze S M 1981 *Physics of Semiconductor Devices* 2nd edn (New York: Wiley)